Microsyst Technol (2012) 18:497–506
DOI 10.1007/s00542-012-1424-1

TECHNICAL PAPER

A new S-shaped MEMS PZT cantilever for energy harvesting from low frequency vibrations below 30 Hz

Huicong Liu · Chengkuo Lee · Takeshi Kobayashi · Cho Jui Tay · Chenggen Quan

Received: 9 December 2011 / Accepted: 2 January 2012 / Published online: 24 January 2012

Abstract In this paper, a new S-shaped piezoelectric PZT cantilever is microfabricated for scavenging vibration energy at low frequencies (<30 Hz) and low accelerations (<0.4g). The maximum voltage and normalized power are 42 mV and 0.31 μW g^{-2}, respectively, at input acceleration of 0.06g. For acceleration above 0.06g, the vibration of PZT cantilever changes from a linear oscillation to a nonlinear impact oscillation due to the displacement constraint introduced by a mechanical stopper. Based on theoretical modeling and experimental results, the frequency broadening effect of the PZT cantilever is studied with varying stop distances and input accelerations. The operation bandwidth of the piezoelectric PZT cantilever is able to extend from 3.4 to 11.1 Hz as the stop distance reduces from 1.7 to 0.7 mm for an acceleration of 0.3g, at the expense of the voltage and normalized power at resonance decreasing from 40 to 16 mV and from 17.8 to 2.8 nW g^{-2}, respectively.

H. Liu · C. J. Tay · C. Quan
Department of Mechanical Engineering,
National University of Singapore,
9 Engineering Drive 1, Singapore 117576, Singapore

C. Lee (✉)
Department of Electrical and Computer Engineering,
National University of Singapore, 4 Engineering Drive 3,
Singapore 117576, Singapore
e-mail: elelc@nus.edu.sg

T. Kobayashi
National Institute of Advanced Industrial Science
and Technology (AIST), 1-2-1 Namiki, Tsukuba,
Ibaraki 305-8564, Japan

1 Introduction

In recent years, the development of low-power-consuming wireless sensor networks has opened up a promising research area on self-powered autonomous sensor nodes by using renewable power sources or energy harvesters to replace the traditional batteries (Starner and Paradiso 2004; Roundy et al. 2003a; Mitcheson et al. 2008). Energy harvesting sources available for wireless sensor networks are mainly solar cells, radio-frequency electromagnetic radiation, thermal gradients and vibrations. Energy harvesting from vibrations has received wide attention since vibration energy is generally a ubiquitous energy source available in ambient, especially where solar or heat energy may not be constantly available, such as buildings or machines. Micro electro mechanical system (MEMS) energy harvesters or scavengers have the advantages of low-volume, low-weight and integration capability with other MEMS components. Generally, there are 3 types of transduction mechanisms (Mitcheson et al. 2004; Beeby et al. 2006), i.e. piezoelectric (Wacharasindhu and Kwon 2008; Yang et al. 2010), electromagnetic (Yang and Lee 2010; Hatipoglu and Urey 2010; Galchev et al. 2011) and electrostatic (Naruse et al. 2009; Lo and Tai 2008), for vibration-based MEMS energy harvesters. By converting mechanical strain into electricity based on direct piezoelectric effect, piezoelectric energy harvesters have received much attention due to the simple configuration and high conversion efficiency (Saadon and Sidek 2001; Anton and Sodano 2007; Tadigadapa and Mateti 2009).

Roundy et al. (2003b) studied some commonly available vibration sources and found that environmental sources have relatively low level of vibration (normally <1g of acceleration) as well as low frequency of vibration (normally <200 Hz). Recently, Miller et al. (2011) have conducted a survey of vibrations available in a machine room of

a large building. The results indicate that the dominant frequency peaks from the majority of the sources surveyed lie between 20 and 60 Hz, and another set of frequencies lies between 120 and 140 Hz. Moreover, the accelerations of the ambient vibrations surveyed are normally below 0.4g. As a result, vibration-based energy harvesters should be able to response to the ambient vibrations with low frequency, low acceleration, and often broadband range. However, most reported piezoelectric MEMS energy harvesters have high resonant frequencies (normally above 200 Hz) (Renaud et al. 2008; Liu et al. 2008; Shen et al. 2009; Elfrink et al. 2009; Lee et al. 2009; Park et al. 2010) or require high acceleration levels (normally above 1g). One study (Miller et al. 2011) has realized energy scavenging at low resonant frequencies of less than 50 Hz with a low acceleration range of 0.03–0.7g.

On the other hand, a traditional linear resonance energy harvester has key features of narrow bandwidth and high quality factor to boost the output voltage and power at its resonant frequency. Such harvester is more practical for the application when the frequency of vibration source is relatively stable. However, for vibration source with random or broadband frequency, even relatively small fluctuations in the ambient vibration frequency will result in significant drops of the output voltage and power of the harvester. With regards to this issue, researchers have presented many energy harvesters with frequency tunable (Leland and Wright 2006; Wu et al. 2008; Challa et al. 2008; Zhu et al. 2010; Eichhorn et al. 2011) and broadband mechanisms. In contrast with frequency tunable energy harvesters, broadband energy harvesters have wide operation bandwidth and do not require extra system or energy to adjust the operation frequency. One way of realizing a broadband operation range is to integrate a series of similar energy harvesters with different resonant frequencies into a system (Xue et al. 2008; Sari et al. 2008). This will result in a wide operation range as well as an increased output power. However, the main drawback of the system is its large size. Another approach is to employ energy harvesters with nonlinear behaviors by the use of magnets (Burrow and Clare 2007), prestressed structures (Marzenki et al. 2009; Tvedt et al. 2010), non-linear springs (Hajaji and Kim 2011; Nguyen and Halvorsen 2011) and mechanical stoppers (Soliman et al. 2008; Blystad and Halvorsen 2010; Gu 2011). For MEMS devices, the use of mechanical stopper mechanism is an attractive solution for achieving a broadband operation range, as it has the advantages of ease of implementation with no additional energy input required. In the authors' previous work (Liu et al. 2011a, b), they have demonstrated a piezoelectric MEMS wideband energy harvester by using mechanical stopper.

In this paper, a new S-shaped piezoelectric PZT cantilever was successfully micro fabricated with small device size and extremely low resonant frequency. Unlike a conventional piezoelectric cantilever which normally contains a straight beam, an S-shaped PZT cantilever is designed for achieving an extremely low resonance of 27.4 Hz. It would be more applicable to ambient vibrations at low frequencies and low accelerations. To the authors' knowledge, no published piezoelectric based energy harvesters have realized such low resonant frequency. In addition, the frequency broadening effect with different stop distances and input accelerations will be studied and discussed based on theoretical modeling and experimental results, which has not been conducted so far.

2 Device configuration

Figure 1a shows a schematic illustration of the piezoelectric PZT cantilever for energy harvesting, which consists of an S-shaped meandering beam connected with a silicon proof mass on the end. The resonant frequency of the spring–mass system is expressed as

$$f = \frac{1}{2\pi}\sqrt{\frac{k}{m}} \tag{1}$$

where k and m represent the effective spring stiffness and the effective mass, respectively. To reduce the resonant frequency, a bulk silicon mass with an area of 2 mm × 1.65 mm and a thickness of 400 μm was employed to achieve a relatively large mass value. In the meantime, an S-shaped meandering beam was configured to reduce the spring stiffness. The meandering beam, which has a piezoelectric coating, comprises of a bottom electrode layer (0.2 μm), a PZT thin film layer (2 μm) and a top electrode layer (0.2 μm). The bottom and top electrodes are connected to their individual bonding pads. The detailed dimensions of the piezoelectric PZT cantilever are shown in Fig. 1b and Table 1. A mode analysis of the PZT cantilever was studied using finite element analysis (FEA) software ABAQUS and a resonant frequency of 27.4 Hz is obtained from the simulation result. When the PZT cantilever is excited by an external vibration, it bends upward and downward resulting in compression and tension of the PZT thin film layer on the meandering beam and consequently generates electrical charges due to the piezoelectric effect.

3 Dynamic modeling

3.1 Linear oscillation system

The piezoelectric PZT cantilever can be modeled as a spring–mass–damping system as shown in Fig. 2a, where the piezoelectric coupling is modeled as a transducer. It

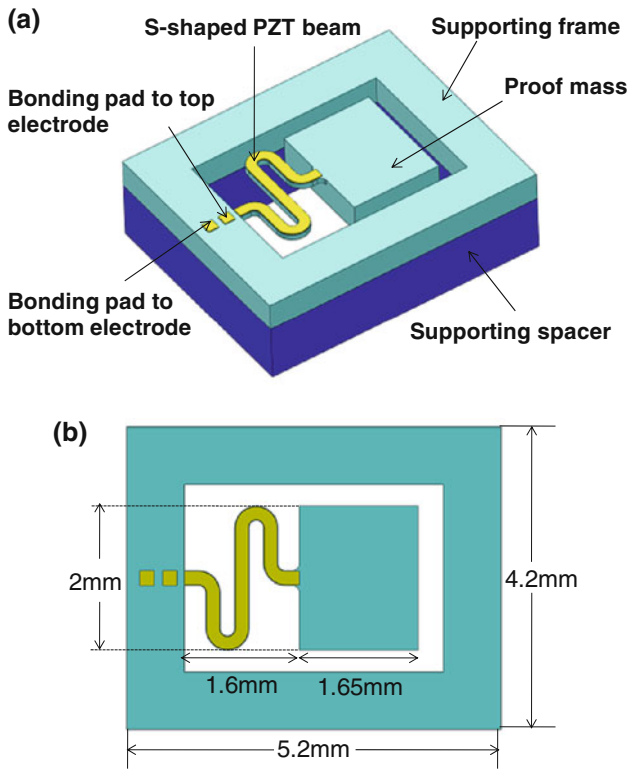

Fig. 1 **a** Schematic drawing of an S-shaped PZT cantilever. **b** Top view of the PZT cantilever device

Table 1 Dimensions of the S-shaped PZT cantilever

Parameters	Descriptions	Values
l	Length of the whole chip	5.2 mm
w	Width of the whole chip	4.2 mm
w_b	Width of the S-shaped beam	0.2 mm
l_b	Actual length of the S-shaped beam	5.2 mm
l_e	Effective length of the S-shaped beam	1.6 mm
l_m	Length of the proof mass	1.65 mm
t_p	Thickness of the PZT layer	2 μm
t_b	Thickness of the S-shaped beam	5 μm
t_m	Thickness of the proof mass	400 μm

consists of an inertial mass (m) suspended by a spring (k_{sp}). The motion of the mass is damped by a parasitic damping (b_m) and a transducer (F_t). When the system is excited by an external displacement $y\ (t)$, the inertial mass moves out of phase with the system base, and the relative displacement is $z\ (t)$.

Applying the Kirchoff's voltage and current laws, the system equations are given by (Roundy and Wright 2004)

$$m\ddot{z} + b_m\dot{z} + k_{sp}z + \frac{c_1 Y d_{31}}{t_p}v = -m\ddot{y} \tag{2}$$

$$\frac{c_2 d_{31} t_p}{\varepsilon}\dot{z} - \frac{1}{RC_p}v = \dot{v} \tag{3}$$

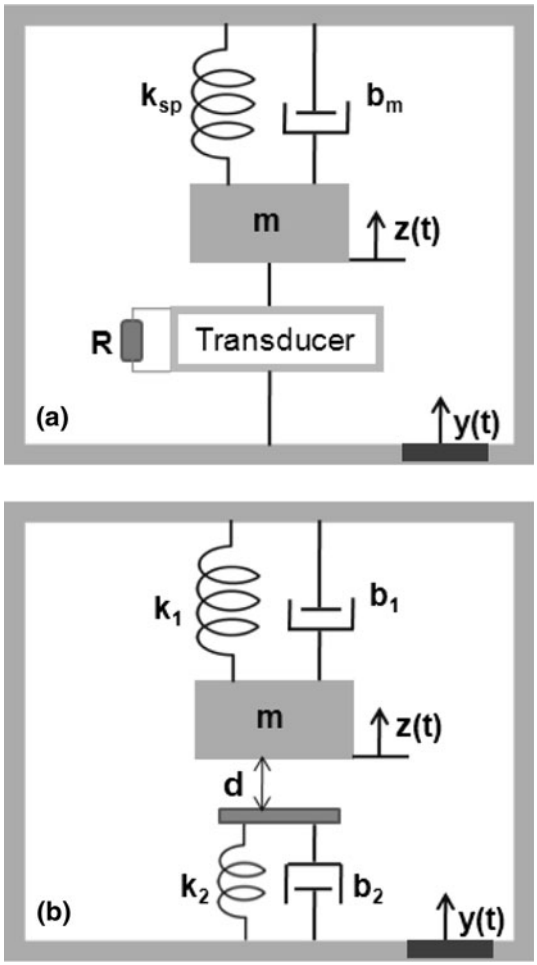

Fig. 2 **a** Mass-spring-damping system of a linear oscillation system. **b** Mechanical model of the oscillation system with mechanical stopper

where v is the output voltage of the load resistor; c_1 is the ratio of the vertical force to the stress in the piezoelectric layer; c_2 is the ratio of the stress in the piezoelectric layer to the vertical displacement of the proof mass; Y is the Young's modulus of the PZT material, i.e. 72.5 GPa; d_{31} is the piezoelectric constant in 31 mode, i.e. -50 pm V^{-1}; ε is the dielectric constant of the PZT material, i.e. 8.85×10^{-9} Fm^{-1}; C_p is the capacitance of the piezoelectric layer, i.e. 3.2 nF; R is the load resistor.

Taking the Laplace transform, the output voltage v is obtained as

$$v = \frac{-j\omega\frac{c_2 d_{31} t_p}{\varepsilon}\ddot{y}}{\left[\frac{1}{RC_p}\omega_n^2 - \left(\frac{1}{RC_p} + 2\varsigma\omega_n\right)\omega^2\right] + j\omega\left[\omega_n^2(1+k^2) + \frac{2\varsigma\omega_n}{RC_p} - \omega^2\right]} \tag{4}$$

where ω is the ambient vibration frequency; ω_n is the resonant frequency of the PZT cantilever; ς is the damping ratio, i.e. 0.006; k is the electromechanical coupling

coefficient represented by $k^2=\frac{Yd_{31}^2}{\varepsilon}$. When the ambient vibration frequency ω matches with the resonant frequency of the PZT cantilever ω_n, Eq. 4 can be simplified as

$$v=\frac{-j\frac{c_2 d_{31} t_p}{\varepsilon}\ddot{y}}{2\varsigma\omega_n^2+j\left(\omega_n^2 k^2+\frac{2\varsigma\omega_n}{RC_p}\right)}. \tag{5}$$

From Eq. 4, the output power P transferred to the load resistor is given by

$$P=\frac{1}{2}\frac{RC_p^2\left(\frac{c_2 d_{31} t_p}{\varepsilon}\right)^2}{(RC_p\omega_n)^2(4\varsigma^2+k^4)+RC_p 4\varsigma\omega_n k^2+4\varsigma^2}\frac{\ddot{y}^2}{\omega_n^2}. \tag{6}$$

3.2 Nonlinear oscillation system with mechanical stopper

Figure 2b illustrates the mechanical model for the oscillation system with one-side mechanical stopper. The differential equation of the mass motion with stopper engaged can be written as

$$\begin{cases}\ddot{z}+2\xi_1\omega_1\dot{z}+\omega_1^2 z=-\ddot{y} & (z>-d)\\ \ddot{z}+(2\xi_1\omega_1+2\xi_2\omega_2)\dot{z}+(\omega_1^2+\omega_2^2)z-\omega_2^2 d=-\ddot{y} & (z\le -d)\end{cases} \tag{7}$$

where $y=Y\sin(\omega t)$, Y is the amplitude of the base excitation, ω is the excitation frequency, ξ_1 and ω_1 are the parasitic damping and frequency characteristics of the oscillation system, i.e. 0.006 and 27.4, ξ_2 and ω_2 are the parasitic damping and frequency characteristics of the stopper, i.e. 0.45 and 118. These parameters can be defined as $2\xi_1\omega_1=\frac{b_1}{m}$, $2\xi_2\omega_2=\frac{b_2}{m}$, $\omega_1^2=\frac{k_1}{m}$, $\omega_2^2=\frac{k_2}{m}$. We use the dimensionless variables $\tau=\omega_1 t, \rho=\frac{\omega}{\omega_1}, \rho_2=\frac{\omega_2}{\omega_1}, u=\frac{z}{Y}, v=\frac{y}{Y}=\sin(r\tau), \delta=\frac{d}{Y}$ to find the following dimensionless equation of the mass motion as

$$\ddot{u}+2\xi_1\dot{u}+u=\rho^2\sin(\rho\tau)+f(u,\dot{u}) \tag{8}$$

where $f(u,\dot{u})=\begin{cases}0 & (u>-\delta)\\ -2\rho_2\xi_2\dot{u}-\rho_2^2 u+\rho_2^2\delta & (u\le-\delta)\end{cases}$

The first-order approximate solution of Eq. 8 is assumed to be

$$u=a(\tau)\sin(\varphi(\tau)) \tag{9}$$

$$\dot{u}=a(\tau)\rho\cos(\varphi(\tau)) \tag{10}$$

$$\varphi(\tau)=\rho\tau+\beta(\tau) \tag{11}$$

where $a(\tau)$ is the slowly varying amplitude, and $\beta(\tau)$ is the slowly varying phase difference between the base excitation and response. Eqs. 9 and 10 imply

$$\dot{a}\sin\varphi+a\dot{\beta}\cos\varphi=0 \tag{12}$$

Substituting Eqs. 9 and 10 into Eq. 8 yields

$$\dot{a}\rho\cos\varphi-a\dot{\beta}\rho\sin\varphi=a(\rho^2-1)\sin\varphi+\rho^2\sin(\varphi-\beta)-2\xi_1 a\rho\cos\varphi+f(u,\dot{u}) \tag{13}$$

Solving Eqs. 12 and 13 for $\dot{a}$ and $\dot{\beta}$, we have

$$\dot{a}\rho=[a(\rho^2-1)+\rho^2\cos\beta]\sin\varphi\cos\varphi-(2\xi_1 a\rho+\rho^2\sin\beta)\cos^2\varphi+f(u,\dot{u})\cos\varphi \tag{14}$$

$$a\dot{\beta}\rho=-[a(\rho^2-1)+\rho^2\cos\beta]\sin^2\varphi+(2\xi_1 a\rho+\rho^2\sin\beta)\cos\varphi\sin\varphi-f(u,\dot{u})\sin\varphi \tag{15}$$

Since the variables $\dot{a}$ and $\dot{\beta}$ change slowly with time, we may suppose that their averages remain constant over a period of 2π. The averaging method was employed to obtain the modulation equations describing the evolution of the amplitude and phase of the mass motion (Narimani et al. 2004). Therefore, the frequency response, i.e. the amplitude a as a function of the excitation frequency ρ, can be found by solving the following Eqs. 16 and 17

$$\pi\rho^2\sin\beta=-2\xi_1 a\rho\pi-\rho_2\xi_2 a\rho(\pi-2\varphi-\sin 2\varphi) \tag{16}$$

$$\pi\rho^2\cos\beta=\pi a(1-\rho^2)-\left[\frac{1}{2}\rho_2^2 a(2\varphi-\sin 2\varphi-\pi)+2\rho_2^2\delta\cos\varphi\right] \tag{17}$$

where $\varphi=\sin^{-1}(\delta/a)$ is the phase angle when the proof mass engages the stopper. Based on Eqs. 16 and 17, the amplitude of the mass motion against excitation frequency can be obtained numerically. Accordingly, the output voltage of the PZT cantilever against excitation frequency can be calculated by Eq. 3.

4 Fabrication and experimental setup

The S-shaped PZT cantilever was fabricated through a micro fabrication process using a silicon-on-insulator (SOI) wafer with 5-μm-thick Si device layer, 1-μm-thick buried oxide layer and 400-μm-thick Si handle layer. The process started from multilayer deposition of Pt/Ti/PZT/Ti/Pt/SiO_2 on the SOI wafer as shown in Fig. 3a. After the thermal oxidation of the SOI wafer at 1,100°C, Pt (0.2 μm)/Ti (0.05 μm) thin films were deposited by DC magnetron sputtering to form the bottom electrode. A Pb ($Zr_{0.52}$, $Ti_{0.48}$) O_3 film of 2.5-μm-thick was then deposited by sol–gel deposition. Finally, Pt (0.2 μm)/Ti (0.05 μm) thin films were deposited by DC magnetron sputtering to form the top electrode. In Fig. 3b, the top and bottom electrodes were etched by Ar ions, and the PZT thin film was wet etched by a mixture of HF, HNO_3 and HCl. A 0.8-μm-thick SiO_2 thin film was then deposited

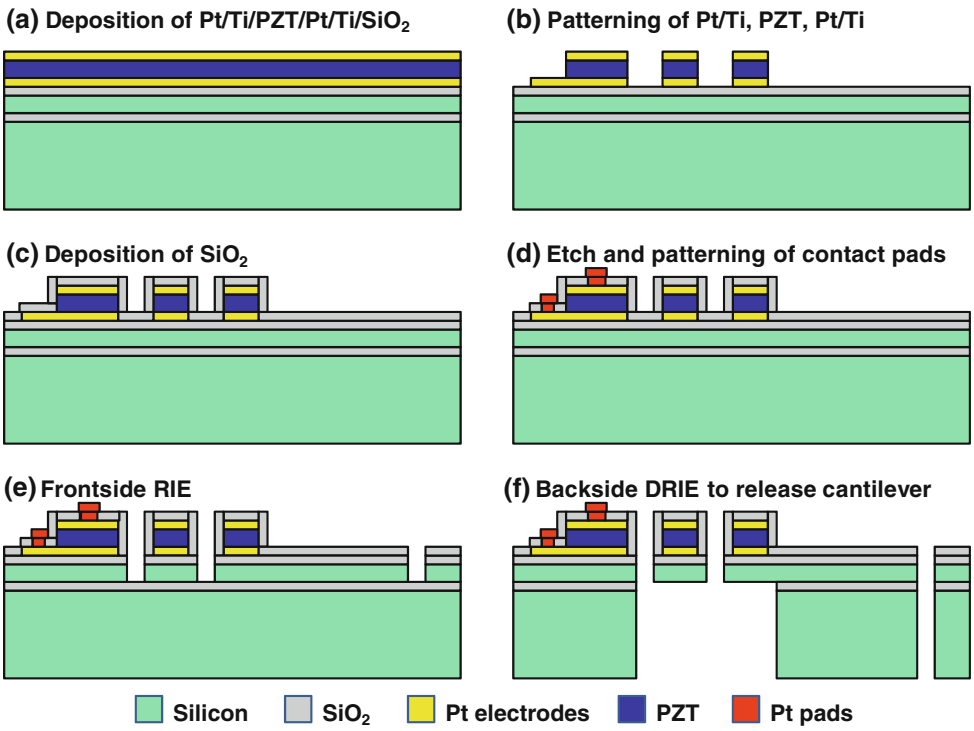

Fig. 3 Microfabrication process of the S-shaped PZT cantilever

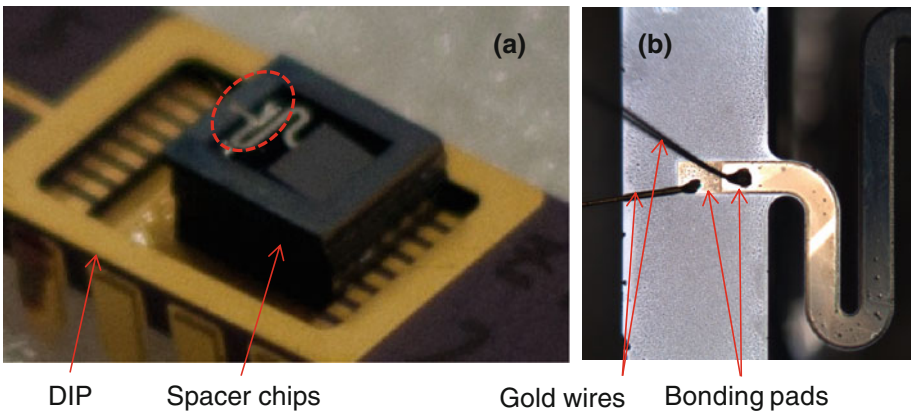

Fig. 4 **a** A packaged MEMS PZT cantilever on a dual in-line package (DIP). **b** Microscopic image of the wire bonding arrangement

by RF-magnetron sputtering as an insulation layer as shown in Fig. 3c. In Fig. 3d, contact holes were etched and patterned with Pt to form the bonding pads. As shown in Fig. 3e, the SiO_2 layer and Si device layer were etched by RIE using feed gases of CHF_3 and SF_6, respectively. Finally, in Fig. 3f, the Si handle layer and buried oxide layer were etched from the backside using DRIE to release the PZT cantilever structure. The micro fabricated device was assembled onto a dual in-line package (DIP) with a spacer chip of 2.1-mm-thick in between as shown in Fig. 4a and the bonding pads are connected to the metal pins of the DIP by gold wires as shown in Fig. 4b.

For the study of the frequency broadening effect of the PZT cantilever with variable stop distances, a stopper adjustment mechanism was employed as shown in Fig. 5a. It is composed of two L-shaped aluminum plates installed on a micro stage, such that the gap in between these two plates can be easily adjusted in the z-direction. The packaged PZT cantilever device was assembled on a breadboard (bottom breadboard) mounted on the bottom L-shaped plate. Another breadboard (top breadboard) was mounted on the top L-shaped plate. A dummy metal package to be used as a mechanical stopper was attached at the top breadboard. With this arrangement, the stop distance between the packaged PZT cantilever device and the mechanical stopper can be finely adjusted.

Figure 5b shows the entire vibration testing system. The assembled mechanism is amounted on a shaker. The vibration frequency and amplitude of the shaker are controlled by a dynamic signal analyzer through an amplifier. The output voltage of the package PZT cantilever device is again collected and recorded by the dynamic signal analyzer. The

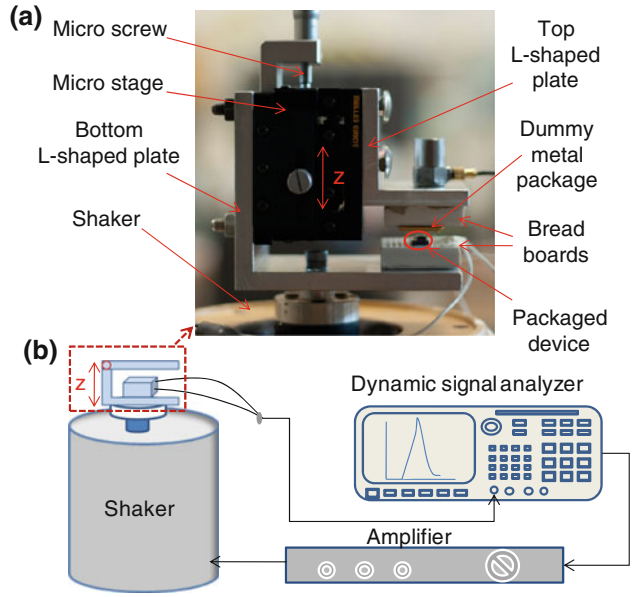

Fig. 5 Experimental setup for the dynamic characterization **a** Assembled stopper adjustment mechanism **b** Vibration testing system

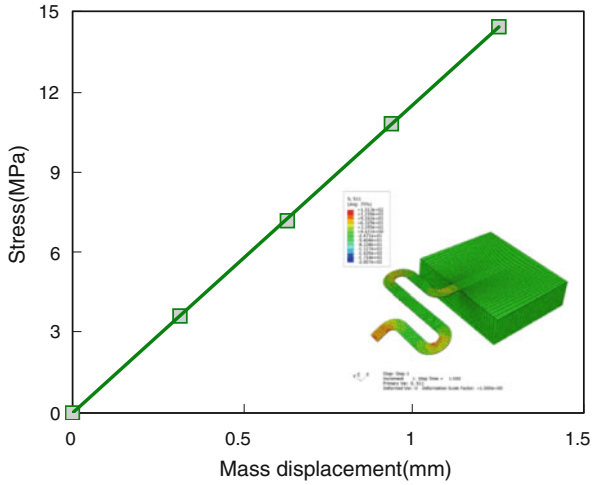

Fig. 6 Relation of the stress in the piezoelectric layer with the vertical displacement of the proof mass

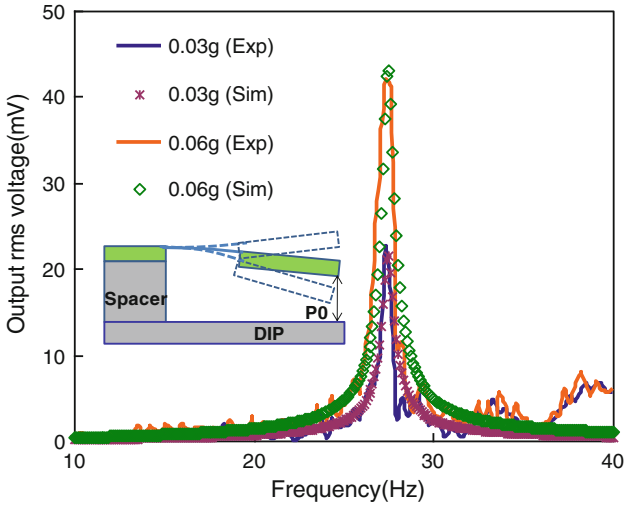

Fig. 7 Numerical and experimental results of output rms voltages against frequency at input accelerations of 0.03 and 0.06*g*

measured output voltage is actually the load rms voltage delivered to the internal impedance of the dynamic signal analyzer, which is assumed to be load resistance of 1 MΩ.

5 Results and discussion

5.1 Linear oscillation without stopper

In the initial state, the proof mass of the PZT cantilever is bended downward duo to the gravitational force. The distance between the bottom surface of the mass tip and the DIP surface is P0 of 1.7 mm. Under low input acceleration, the vibration of the PZT cantilever is not sufficient to impact the DIP and hence it is considered as a linear oscillation. For a linear oscillation system, the output voltage can be obtained numerically using Eq. 4. The ratio c_2 of the stress in the piezoelectric layer to the vertical displacement of the proof mass is obtained by using FEA simulation software ABAQUS. Here simulated body forces of 1, 2, 3 and 4*g* were applied to the PZT cantilever model, with fixed condition at the anchor of the S-shape beam. The corresponding mass vertical displacements versus the average stresses were shown in Fig. 6 and the ratio c_2 can be obtained subsequently. Figure 7 shows the numerical modeling and experimental results of the output voltages against frequency at input accelerations of 0.03 and 0.06*g*. The experimental results show maximum output voltages of 22.5 and 42.1 mV which occur at its resonant frequency of 27.4 Hz at relatively low input accelerations of 0.03 and 0.06*g*, respectively. It is seen that the simulation results agree well with the experimental results. For an acceleration of 0.06*g*, the rms voltage and power against load resistance at resonant frequency of 27.4 Hz are simulated using Eqs. 5, 6 and shown in Fig. 8. As can be expected, under such a low input acceleration of 0.06*g*, a maximum power of 1.117 nW, which is 0.31 μW g^{-2} in terms of normalized power, is generated at the optimum load resistance of 1.6 MΩ and its resonance of 27.4 Hz.

5.2 Nonlinear impact oscillation with variable stopper

As the top variable stopper is engaged, the vibration of PZT cantilever transforms from a linear oscillation to a nonlinear impact oscillation due to the displacement constraint given by the mechanical stopper. The operation-frequency of such

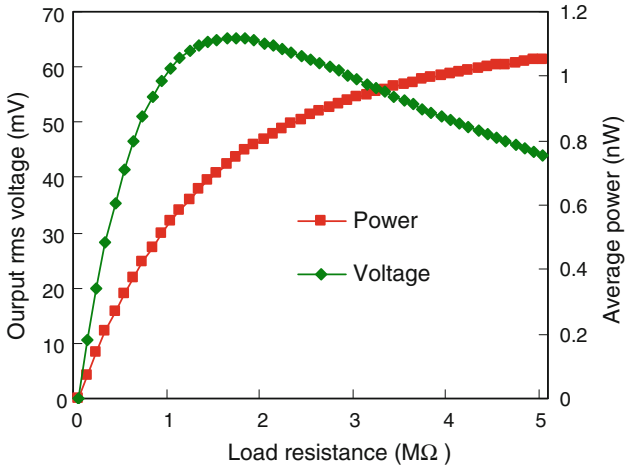

Fig. 8 Simulated results of the output rms voltage and power against load resistance at resonance of 27.4 Hz

nonlinear impact oscillation system exhibits a broad bandwidth in the neighborhood of its resonant frequency, which is named as frequency broadening effect. This is because when the PZT cantilever engages the stopper, the responses diverge from each other and the effective stiffness of the system increases abruptly. The higher effective stiffness increases the effective natural frequency beyond ω_n causing resonance to extend over a wider interval of the frequency spectrum (Narimani et al. 2004; Soliman et al. 2008). The stiffness increase is in proportion to the excursion size and the interval of the engagement per cycle. Hence, higher input acceleration and lower stop distance will induce a wider operation bandwidth.

The stop distances between the top surface of proof mass and the top stopper are set at P1 (1.7 mm), P2 (1.2 mm) and P3 (0.7 mm) as shown in Fig. 9. For each stop distance, frequency up-sweeps and down-sweeps were performed under input accelerations of A1 (0.1 g), A2 (0.2 g) and A3 (0.3g). Fig. 10 shows the output rms voltage against frequency for various stop distances and input accelerations. In Fig. 10a, "A1_P1_U" and "A1_P1_D" represent the case

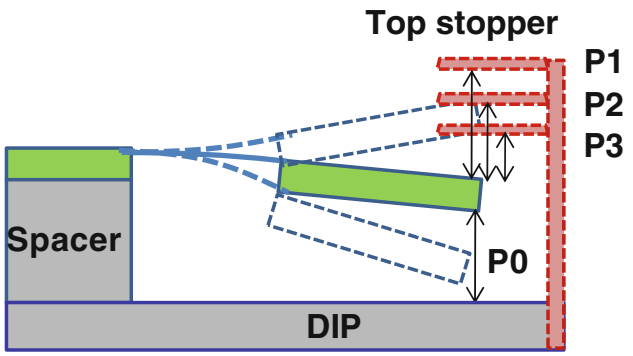

Fig. 9 Configuration of the PZT cantilever device with an adjustable top stopper

of acceleration (A1), stop distance (P1) and frequency up-sweep (U) or down-sweep (D). The corresponding legends are also indicated in Fig. 10b–i and Table 2 summarizes the frequency sweeps (up-sweeps) response under various situations, where f_l shows the frequency when the top stopper is engaged; f_r represents the frequency where the output rms voltage drops dramatically; Δf is the operation frequency bandwidth from f_l to f_r; V_r is the output rms voltage at resonance of 27.4 Hz; P_r/a^2 is the corresponding power normalized by input acceleration (normalized power).

For input acceleration of 0.2g, the output voltages against frequencies are simulated numerically using Eqs. 3, 16, 17 with stop distances varying from P1 to P3, as shown in Fig. 11. The parameters used in the modeling can be referred to Sect. 3. For comparison, the corresponding experimental results are plotted in the same figure, where "S" and "E" represent simulation and experimental results, respectively. As can be seen, the quantitative estimation of the output voltage and broadening frequency range are in good agreement with the experimental results.

Based on the simulation and experimental results, it can be found that for a given stop distance, the up-sweep bandwidth of the nonlinear impact oscillation system is broadened as the input acceleration increases. The output voltage is relative constant though it shows a slightly increasing trend within the operation bandwidth. For example, for a stop distance of P2, the operation bandwidth increases from 2.6 to 6.0 Hz as the input acceleration increases from A1 to A3, while the output voltage at resonance remains relatively constant at around 28 mV and the normalized power at resonance decreases from 78.4 to 9.3 nW g^{-2}. On the other hand, for a given input acceleration, the output voltage is suppressed by the stopper and thus decreases gradually as the stop distance decreases from P1 to P3. However, the up-sweep bandwidth is broadened as the stop distance decreases at the expense of lower voltage and power output. For instance, for an input acceleration of A3, the output voltage and the normalized power at resonance are decreased from 40 to 16 mV and from 17.8 to 2.8 nW g^{-2} when the stop distance is reduced from P1 to P3. The frequency bandwidth however is increased from 3.4 to 11.1 Hz. For a down-sweep bandwidth in the case of the nonlinear impact oscillation system, the operation frequency remains similar to that of the system without a stopper at any given stop distances and input accelerations.

From the above discussion, it is seen that a broadening effect of the PZT cantilever can be realized by utilizing mechanical stopper mechanism. The broadening effect is strongly influenced by the stop distance and input acceleration. For a given stop distance, the operation bandwidth increases with the input acceleration. While for a given input acceleration, the operation bandwidth increases with a decrease in the stop distance. However, a smaller stop

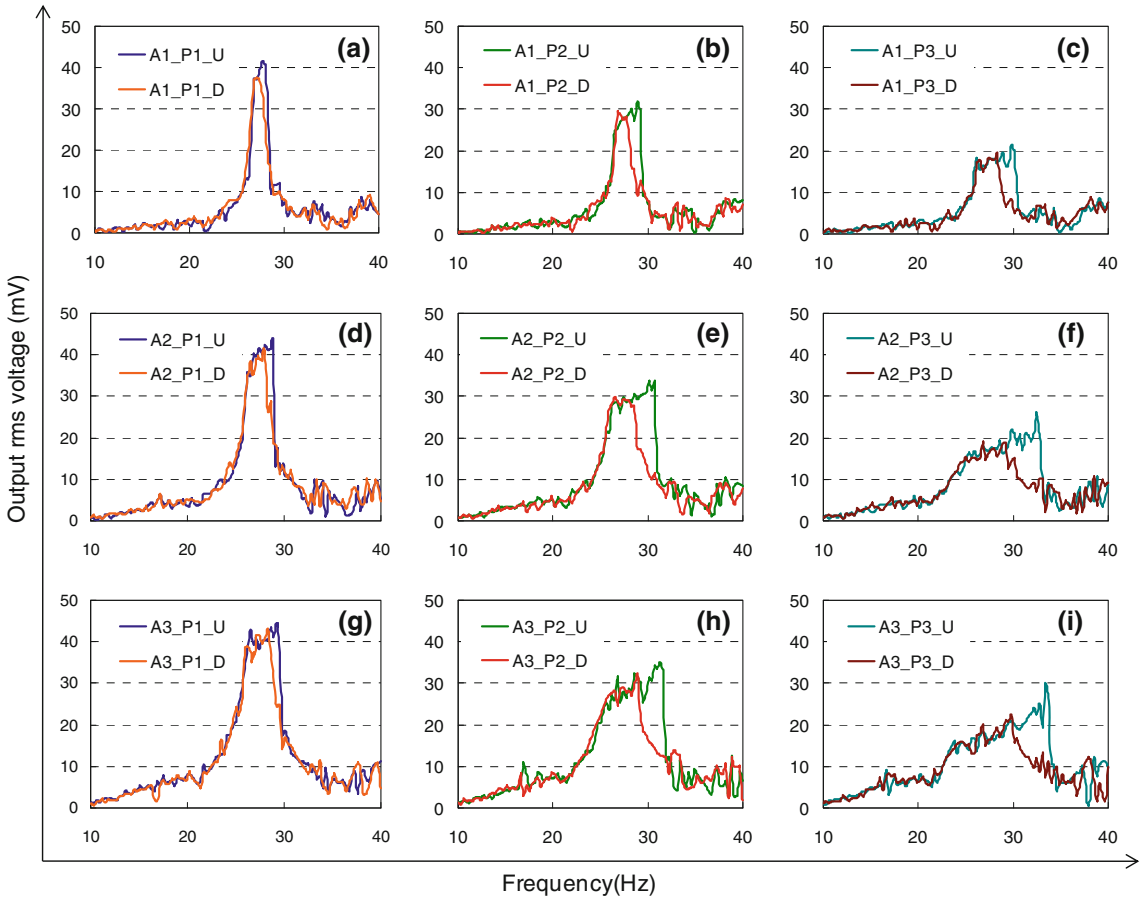

Fig. 10 Output rms voltages against frequency with various stop distances (*P1*, *P2* and *P3*) and input accelerations (*A1, A2* and *A3*)

Table 2 Summary of the frequency up-sweeps response under various situations

	P1					P2					P3				
	f_1 (Hz)	fr (Hz)	Δf (Hz)	V_r (mV)	P_r/a^2 (nW g^{-2})	f_1 (Hz)	fr (Hz)	Δf (Hz)	V_r (mV)	P_r/a^2 (nW g^{-2})	f_1 (Hz)	fr (Hz)	Δf (Hz)	V_r (mV)	P_r/a^2 (nW g^{-2})
A1	26.9	28.0	1.1	37	136.9	26.6	29.2	2.6	28	78.4	26	30.2	4.2	18	32.4
A2	26.2	29.0	2.8	38	36.1	25.9	30.1	4.2	29	21.0	25.1	32.9	7.8	17	7.225
A3	25.8	29.5	3.4	40	17.8	25.6	31.6	6.0	29	9.3	23.5	33.6	11.1	16	2.8

distance will also result in a lower output voltage and power. Therefore, there is a trade-off between the operation bandwidth and output power for such nonlinear impact oscillation system. An optimization procedure should be implemented according to the requirements of the applications.

Because of the low operating frequency and small PZT pattern area, the output power of the S-shaped PZT cantilever is not significant. As a future work, it is proposed to replace the mechanical stopper with a piezoelectric cantilever with high resonant frequency and large PZT pattern area. The high-frequency piezoelectric cantilever can be excited and self-oscillated due to the impact caused by the low-frequency S-shaped PZT cantilever which responses to low frequency vibrations. With so-called frequency-up-conversion technique (Sari et al. 2010), the output power of the system is expected to be boosted significantly.

6 Concluding remarks

In this paper, we provide a new MEMS piezoelectric energy harvester with S-shaped PZT cantilever to bring down the operating frequency below 30 Hz. The vibration behavior of the PZT cantilever is studied based on linear oscillation as well as nonlinear impact oscillation. For the

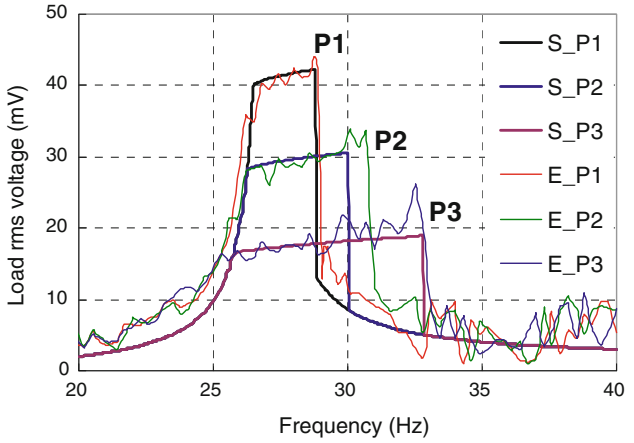

Fig. 11 Simulated and experimental results of the output rms voltages against frequency with various stop distances (*P1, P2* and *P3*) and input accelerations of 0.2*g*

nonlinear oscillation system with variable stopper, the broadened operation bandwidth was characterized for various input accelerations and stop distances. The operation bandwidth of the system is broadened as the stop distance decreases at the expense of lower output voltage and power. With further improvement of output power by using high-frequency piezoelectric cantilever stopper, this kind of energy harvester could be a design to scavenge energy from vibrations at frequencies less than 30 Hz.

Acknowledgments This work was partially supported in research grant of Academic Research Committee Fund MOE2009-T2-2-011 (R-263000598112) and AcRF Tier 1-FRC (Project Title: MEMS Energy Harvesting Mechanisms for Collecting Energy from Vibrations) at the National University of Singapore.

References

Anton SR, Sodano HA (2007) A review of power harvesting using piezoelectric materials (2003–2006). Smart Mater Struct 16:R1–R21

Beeby SP, Tudor MJ, White NM (2006) Energy harvesting vibration sources for microsystems applications. Meas Sci Technol 17:175–195

Blystad L-CJ, Halvorsen E (2010) A piezoelectric energy harvester with a mechanical end stop on one side. Microsyst Technol 17:505–511

Burrow SG, Clare LR (2007) A resonant generator with non-linear compliance for energy harvesting in high vibrational environments. In: IEEE International Electric Machines and Drives Conference, pp 715–720

Challa VR, Prasad MG, Shi Y, Fisher FT (2008) A vibration energy harvesting device with bidirectional resonance frequency tenability. Smart Mater Struct 17:015035

Eichhorn C, Tchagsim R, Wilhelm N, Woias P (2011) A smart and self-sufficient frequency tunable vibration energy harvester. J Micromech Microeng 21:104003

Elfrink R, Kamel TM, Goedbloed M, Matova S, Hohlfeld D, van Andel Y, van Schaijk R (2009) Vibration energy harvesting with aluminum nitride-based piezoelectric devices. J Micromech Microeng 19:094005

Galchev T, Kim H, Najafi K (2011) Micro power generator for harvesting low-frequency and nonperiodic vibrations. J Microelectromech Sys 20:852–866

Gu L (2011) Low-frequency piezoelectric energy harvesting prototype suitable for the MEMS implementation. Microelectron J 42:277–282

Hajaji A, Kim S-G (2011) Ultra-wide bandwidth piezoelectric energy harvesting. Appl Phys Lett 99:083105

Hatipoglu G, Urey H (2010) FR4-based electromagnetic energy harvester for wireless sensor nodes. Smart Mater Struct 19:015022

Lee BS, Lin SC, Wu WJ, Wang XY, Chang PZ, Lee CK (2009) Piezoelectric MEMS generators fabricated with an aerosol deposition PZT thin film. J Micromech Microeng 19:065014

Leland ES, Wright PK (2006) Resonance tuning of piezoelectric vibration energy scavenging generators using compressive axial preload. Smart Mater Struct 15:1413–1420

Liu JQ, Fang HB, Xu ZY, Mao XH, Shen XC, Chen D, Liao H, Cai BC (2008) A MEMS-based piezoelectric power generator array for vibration energy harvesting. Microelectron J 39:802–806

Liu H, Tay CJ, Quan C, Kobayashi T, Lee C (2011a) Piezoelectric MEMS energy harvester for low-frequency vibrations with wideband operation range and steadily increased output power. J Microelectromech Syst 20(5):1131–1142

Liu H, Tay CJ, Quan C, Kobayashi T, Lee C (2011b) A scrape-through piezoelectric MEMS energy harvester with frequency broadband and up-conversion behaviors. Microsyst Technol 17:1747–1754

Lo H, Tai Y (2008) Parylene-based electrets power generators. J Micromech Microeng 18:104006

Marzenki M, Defosseux M, Basrour S (2009) MEMS vibration energy harvesting devices with passive resonance frequency adaption capability. J Microelectromech Syst 18:1444–1453

Miller LM, Halvorsen E, Dong T, Wright PK (2011) Modeling and experimental verification of low-frequency MEMS energy harvesting from ambient vibrations. J Micromech Microeng 21:045029

Mitcheson PD, Green TC, Yeatman EM, Holmes AS (2004) Architectures for vibration-driven micropower generators. J Microelectromech Syst 13:429–440

Mitcheson PD, Yeatman EM, Rao GK, Holmes AS, Green TC (2008) Energy harvesting from human and machine motion for wireless electronic devices. Proc IEEE 96:1457–1486

Narimani A, Golnaraghi MF, Jazar GN (2004) Frequency response of a piecewise linear vibration isolator. J Vib Control 10:1775–1794

Naruse Y, Matsubara N, Mabuchi K, Izumi M, Suzuki S (2009) Electrostatic micro power generation from low-frequency vibration such as human motion. J Micromech Microeng 19:094002

Nguyen SD, Halvorsen E (2011) Nonlinear springs for bandwidth-tolerant vibration energy harvesting. J Microelectromech Syst 20(6):1225–1227

Park JC, Park JY, Lee Y-P (2010) Modeling and characterization of piezoelectric d33-mode MEMS energy harvester. J Microelectromech Syst 19:1215–1222

Renaud M, Karakaya K, Sterken T, Fiorini P, Van Hoof C, Puers R (2008) Fabrication, modeling and characterization of MEMS piezoelectric vibration harvesters. Sens Actuators Phys 145–146:380–386

Roundy S, Wright PK (2004) A piezoelectric vibration based generator for wireless electronics. Smart Mater Struct 13:1131–1142

Roundy S, Wirght PK, Rabaey JM (2003a) Energy scavenging for wireless sensor networks, 1st edn. Kluwer academic, Boston

Roundy S, Wright PK, Rabaey J (2003b) A study of low level vibrations as a power source for wireless sensor nodes. Comput Commun 26:1131–1144

Saadon S, Sidek O (2001) A review of vibration-based MEMS piezoelectric energy harvesters. Energy Convers Manage 52:500–504

Sari I, Balkan T, Kulah H (2008) An electromagnetic micro power generator for wideband environmental vibrations. Sens Actuators Phys 145–146:405–413

Sari I, Balkan T, Kulah H (2010) An electromagnetic micro power generator for low-frequency environmental vibrations based on the frequency up conversion technique. J Microelectromech Syst 19:14–27

Shen D, Park J-H, Noh JH, Choe S-Y, Kim S-H, Wikle HC III, Kim D-J (2009) Micromachined PZT cantilever based on SOI structure for low frequency vibration energy harvesting. Sens Actuators Phys 154:103–108

Soliman MSM, Abdel-Rahman EM, El-Saadany EF, Mansour RR (2008) A wideband vibration-based energy harvester. J Micromech Microeng 18:115021

Starner T, Paradiso JA (2004) Human generated power for mobile electronics. In: Piquet C (ed) Low-power electronics design. CRC Press, Boca Raton pp 1–35

Tadigadapa S, Mateti K (2009) Piezoelectric MEMS sensors: state-of-the-art and perspectives. Meas Sci Technol 20:092001

Tvedt LGW, Nguyen DS, Halvorsen E (2010) Nonlinear behavior of an electrostatic energy harvester under wide- and narrowband excitation. J Microelectromech Syst 19:305–316

Wacharasindhu T, Kwon JW (2008) A micromachined energy harvester from a keyboard using combined electromagnetic and piezoelectric conversion. J Micromech Microeng 18:104016

Wu X, Lin J, Kato S, Zhang K, Ren T, Liu L (2008) A frequency adjustable vibration energy harvester. In: Proceedings of PowerMEMS 2008 + microEMS 2008, pp 245–248

Xue H, Hu Y, Wang QM (2008) Broadband piezoelectric energy harvesting devices using multiple bimorphs with different operating frequencies. IEEE Trans Ultrason Ferroelectr Freq Control 55:2104–2108

Yang B, Lee C (2010) Non-resonant electromagnetic wideband energy harvesting mechanism for low frequency vibrations. Microsyst Technol 16:961–966

Yang B, Lee C, Kee WL, Lim SP (2010) Hybrid energy harvester based on piezoelectric and electromagnetic mechanisms. J Micro/Nanolith MEMS MOEMS 9:023002

Zhu D, Roberts S, Tudor MJ, Beeby SP (2010) Design and experimental characterization of a tunable vibration-based electromagnetic micro-generator. Sens Actuators Phys 158:284–293